



City Research Online

City, University of London Institutional Repository

Citation: Nguyen, K., Camara, A., Rio, O. & Sparowitz, L. (2017). Dynamic Effects of Turbulent Crosswind on the Serviceability State of Vibrations of a Slender Arch Bridge Including Wind-Vehicle-Bridge Interaction. *Journal of Bridge Engineering*, 22(11), 06017005. doi: 10.1061/(asce)be.1943-5592.0001110

This is the accepted version of the paper.

This version of the publication may differ from the final published version.

Permanent repository link: <https://openaccess.city.ac.uk/id/eprint/18175/>

Link to published version: [https://doi.org/10.1061/\(asce\)be.1943-5592.0001110](https://doi.org/10.1061/(asce)be.1943-5592.0001110)

Copyright: City Research Online aims to make research outputs of City, University of London available to a wider audience. Copyright and Moral Rights remain with the author(s) and/or copyright holders. URLs from City Research Online may be freely distributed and linked to.

Reuse: Copies of full items can be used for personal research or study, educational, or not-for-profit purposes without prior permission or charge. Provided that the authors, title and full bibliographic details are credited, a hyperlink and/or URL is given for the original metadata page and the content is not changed in any way.

City Research Online:

<http://openaccess.city.ac.uk/>

publications@city.ac.uk

Cite as:

Nguyen K, Camara A, Rio O, Sparowitz L (2017), Dynamic effects of turbulent crosswind on the serviceability state of vibrations of a slender arch bridge including wind-vehicle-bridge interaction. Journal of Bridge Engineering. Technical Note. 22(11): 06017005.

Dynamic effects of turbulent crosswind on the serviceability state of vibrations of a slender arch bridge including wind-vehicle-bridge interaction

K. Nguyen ¹, A. Camara ² O. Rio ³, L. Sparowitz ⁴

ABSTRACT

1 The use of high performance materials in bridges is leading to structures that are
2 more susceptible to wind- and traffic-induced vibrations due to the reduction in the
3 weight and the increment of the slenderness in the deck. Bridges can experience con-
4 siderable vibration due to both moving vehicles and wind actions that affect the comfort
5 of the bridge users and the driving safety. This work explores the driving safety and
6 comfort in a very slender arch bridge under turbulent wind and vehicle actions, as well
7 as the comfort of pedestrians. A fully coupled wind-vehicle-bridge interaction model
8 based on the direct integration the system of dynamics is developed. In this model, the
9 turbulent crosswind is represented by means of aerodynamic forces acting on the vehicle

¹Department of Continuum Mechanics and Structure Theories, School of Civil Engineering,
Technical University of Madrid, Madrid, Spain. Email: khanh@mecanica.upm.es

²Department of Civil Engineering, School of Mathematics, Computer Science & Engineering,
City University of London, UK. Email: Afredo.camara@city.ac.uk

³Former researcher of department of Construction, Eduardo Torroja Institute for Construc-
tion Science - CSIC, Serrano Galvache No 4, 28033, Madrid, Spain. Email: rio@ietcc.csic.es

⁴Laboratory for Structural Engineering, Graz University of Technology, Graz, Austria.
Email: lutz.sparowitz@tugraz.at

10 and the bridge. The vehicle is modelled as a multibody system that interacts with the
11 bridge by means of moving contacts that also simulate the road surface irregularities.
12 An user element is presented with generality and implemented using a general-purpose
13 finite element software package in order to incorporate the aeroelastic components of
14 the wind forces, which allows to model and solve the wind-vehicle-bridge interaction in
15 time domain without the need of using the modal superposition technique. An exten-
16 sive computational analysis programme is performed on the basis of a wide range of the
17 turbulent crosswind speeds. The results show that the bridge vibration is significantly
18 affected by the crosswind in terms of the peak acceleration and the frequency content
19 when the intensity crosswind is significant. The crosswind has more effect on the ride
20 comfort of the vehicle in lateral direction, and consequently on its safety in terms of
21 overturning accidents.

Keywords: turbulent wind, wind-vehicle-bridge-interaction, serviceability limit
state of vibrations, human response to vibrations

22 INTRODUCTION

23 The concern about wind and traffic-induced vibrations of structures have in-
24 creased in recent years. Road vehicles can be exposed to accident risks when
25 crossing a location where the topographical features magnify the wind effects,
26 such as bridges located in wind-prone regions. The recent advent of high-strength
27 materials is leading to slender bridges that experience significant vibrations un-
28 der moving vehicles and turbulent winds. Therefore, the comfort and safety of
29 the bridge users (pedestrians and vehicle users) are important issues that cannot
30 be neglected in the design of slender bridges. Recent studies in this field have
31 been mainly focused on the driving comfort and safety of the vehicle running on
32 the ground or in long span cable-supported bridges with conventional materials
33 ([Cai and Chen 2004](#); [Xu and Guo 2004](#); [Chen and Cai 2004](#); [Guo and Xu 2006](#);
34 [Snæbjörnsson et al. 2007](#); [Sterling et al. 2010](#); [Zhou and Chen 2015](#)). Unfor-

35 tunately, there is a clear lack of applications to other slender structures such
36 as arch bridges. Furthermore, the comfort of other users of the bridge, such as
37 pedestrians, has been routinely ignored.

38 In order to ensure the users' comfort, most codes and standards establish the
39 design criteria for the Serviceability Limit State (SLS) of vibrations, in which two
40 types of analysis procedures can be classified: deflection- and acceleration-based
41 methods. The first one intends to control the bridge vibration by limiting the
42 bridge deflection under a the static load. This is the approach followed by the
43 American Association State Highway Transportation Officials (AASHTO) ([Amer-](#)
44 [ican Association of State Highway and Transportation Officials 1998](#)), which spec-
45 ifies a deflection criteria of $L/800$ for vehicular bridges and $L/1000$ for bridges
46 with footpaths. Other criteria established in standards and guidelines ([BS 5400-](#)
47 [2:2006 2006](#); [RPX-95 1995](#)) uses a value calculated from the fundamental fre-
48 quency of bridge. However, researchers and practitioners widely recognize that
49 deflection limits are not appropriate for controlling the bridge vibrations ([Wright](#)
50 [and Walker 2004](#); [Azizinamini et al. 2004](#); [Roeder et al. 2004](#)).

51 From the point of view of human comfort, the acceleration-based methods
52 seem to be more rational because the human response depends on the character-
53 istics of the excitation ([Griffin 1990](#)). Some codes ([BS 5400-2:2006 2006](#); [RPX-95](#)
54 [1995](#)) propose a limit of the peak vertical acceleration $a_{lim} = 0.5\sqrt{f_0}$ (f_0 is the
55 fundamental frequency of structure in Hz) for both footbridges and road bridges
56 with footpath, but the use of this value is questionable. The acceleration of the
57 deck nearby the abutments would far exceed the admissible limit when the vehicle
58 enters and leaves the bridge ([Moghimini and Ronagh 2008](#); [Nguyen et al. 2015](#)).
59 This limit can also be easily exceeded anywhere on the deck if the pavement irreg-
60 ularities are large ([Camara et al. 2014](#); [Nguyen et al. 2015](#)). Additionally, ([Boggs](#)
61 [and Petersen 1995](#)) observed that the application of some laboratory test results

62 based on the peak acceleration results in unrealistically severe evaluations in real
 63 buildings which are inconsistent with observation. The Root Mean Square (RMS)
 64 acceleration seems to be the most appropriate index in the context of the evalu-
 65 ation of human comfort. In fact, the ISO 2631 ([ISO 2631-1:1997 1997](#)) and the
 66 BS 6841:1987 ([BS 6841:1987 2012](#)) propose the use of weighted RMS acceleration
 67 in vibration evaluation. However, no specified limit of weighted RMS accelera-
 68 tion is defined in these codes in order to assess the comfort. Furthermore, the
 69 human response to vibration depends not only on the exposure time, magnitude
 70 and direction of excitation, human posture, but also on the frequency content
 71 of the vibration. In this sense, the frequency weighting curve is widely used to
 72 incorporate the frequency-related human perception to the comfort evaluation.
 73 Irwin ([Irwin 1978](#)) suggested base curves for acceptable human response to the
 74 vibration of a bridge for both vertical and lateral direction. On the other hand,
 75 the ISO 2631 ([ISO 2631:1978 1978](#)) defines three distinct limit curves for whole-
 76 body vibration for different levels of exposure time (see Fig. III): i) exposure
 77 limits (concerned with the preservation of health or safety), ii) fatigue-decreased
 78 proficiency boundary (concerned with the preservation of working efficiency) and
 79 iii) reduced comfort boundary (concerned with the preservation of comfort). The
 80 vibration levels below the base curves are regarded as comfortable and those
 81 above these curves are considered uncomfortable. In the present investigation,
 82 the Irwin's curves for vertical and lateral bridge vibration in storm conditions
 83 are selected as base curves to assess the pedestrians' comfort, while the fatigue-
 84 decreased proficiency boundaries for 1-min exposure time are used as the base
 85 curve for the ride comfort evaluation of vehicle users.

86 In the last decades, there have been many comprehensive studies based on
 87 frequency- and time-domain analyses to estimate the wind-induced buffeting re-
 88 sponse of bridges ([Davenport 1962](#); [Scanlan 1978](#); [Miyata and Yamada 1990](#); [Chen](#)

et al. 2000; Xu et al. 2000; Xu and Guo 2003; Cai and Chen 2004). Favoured by the linear and elastic response of the bridges, almost all the studies are based on the modal superposition technique. This requires advanced coding skills to solve the coupled dynamic wind-vehicle-bridge interaction, which is hindering its widespread application by engineering practitioners and researchers. With the advancement of Finite Element (FE) methods and computing technologies, a variety of FE software, such as Abaqus, Ansys or Nastran have been widely applied to various disciplines. These software packages combine a friendly graphical user interface and powerful computational capabilities. One of the main difficulties of using commercial FE programs for wind engineering studies is the definition of the aeroelastic effects due to the dependence with the instantaneous deformed configuration, which is not included in standard distribution packages.

This work develops a new type of element that can be applied with generality to any commercial software in order to represent the aeroelastic components of wind forces. The proposed fully coupled wind-vehicle-bridge interaction model allows the direct time-domain integration of the system of dynamics which can be used to consider nonlinear effects such as the loss of contact between the wheels and the pavement, among others. This model is applied in an extensive analysis programme to assess the driving safety and users' comfort in a very slender arch bridge made of Ultra-High Performance Fiber-Reinforced concrete, focusing on the users comfort subject to turbulent crosswind.

THE BRIDGE AND ITS PAVEMENT

The Wild Bridge (Sparowitz et al. 2011) is part of the new Eastern access of Völkermakt (Austria) and uses Ultra High Performance Fiber Reinforced Concrete (UHPFRC), which confers design a remarkable slenderness and light-weight. The arched structure is adopted due to the shape of the valley as shown in Figure

115 2. Detailed description of this bridge can be found in (Nguyen et al. 2015).

116 A three-dimensional finite element model of the Wild Bridge was developed
117 in Abaqus (SIMULIA 2011). The deck, arches and piers were modelled by means
118 of three-dimensional beam elements. Some auxiliary surface elements are intro-
119 duced in the model to materialize the deck surface. These elements do not have
120 inherent stiffness and mass and are constrained rigidly to the deck beam elements,
121 therefore, these elements are only used for establishing the contact between the
122 tire element and the deck surface and distribute the forces to the beam elements.
123 Multi-point constraints were used to impose the kinematic relationship between
124 the node of the pier and the corresponding node of the deck in order to model the
125 fixed connection between both. The deck is connected to the abutments by four
126 elastomeric bearings (EBs) of $350 \times 300 \times 126$ mm that allow vertical and horizon-
127 tal displacements. Each EB was modelled by means of linear springs representing
128 the vertical and horizontal stiffness, according to (CEN 2005a).

129 The mechanical properties of the materials employed in different parts of
130 the bridge have been obtained from the modal updating of site measurements
131 conducted in a precursor work (Nguyen et al. 2015). These are summarized in
132 the Table 1, including its designation, adopted and updated value, respective unit
133 and references. The frequencies of the first six modes of vibration of the bridge
134 are listed in the Table 2.

135 In this study, we focus on the study of the wind effects on the vehicle-bridge
136 vibration, however, the road surface always has some geometric imperfections. In
137 order to take this into account in the vehicle-bridge interaction, a road surface
138 roughness is defined. Appropriate road roughness profiles under the left and
139 right wheels are generated so that there is an adequate coherence between them
140 accepting the hypothesis of the isotropy of the road surface (Dodds and Robson
141 1973; Kamash and Robson 1978). The road roughness profile is generated as a

142 zero-mean stationary Gaussian random process and can be generated as the sum
 143 of a series of harmonics:

$$r_1(x) = \sum_{i=1}^N \sqrt{2G(n_i)\Delta n} \cos(2\pi n_i x + \phi_i) \quad (1)$$

144 and the second parallel profile at distance $2b$ is defined by (Sayers 1988):

$$r_2(x) = \sum_{i=1}^N (\sqrt{2G(n_i)\Delta n} \cos(2\pi n_i x + \phi_i) + \sqrt{2(G(n_i) - G_x(n_i))\Delta n} \cos(2\pi n_i x + \theta_i)) \quad (2)$$

145 in which N is the number of discrete frequencies n_i in range $[n_{min}, n_{max}]$, Δn is the
 146 increment between successive frequencies, ϕ_i is the random phase angle uniformly
 147 distributed from 0 to 2π , θ_i is other random uniformly distributed phase angles.
 148 $G(n)$ and $G_x(n)$ are the one-sided direct and cross power spectral density (PSD)
 149 functions, respectively. In this work, the PSD value at a reference frequency of
 150 0.1 cycle/m is defined as $64 \times 10^{-3} \text{ m}^3$ that corresponds to the “good” quality
 151 of road surface. A range of frequency of interest from 0.01 to 10 cycle/m as
 152 recommended by ISO 8608:1995 (ISO 8608:1995 1995) were also considered in
 153 this work.

154 THE VEHICLE

155 The high-sided truck model shown in Fig. 3 is considered in this work as
 156 it combines large velocities and exposed areas to wind. This vehicle model is
 157 consistent a large number of previous works (Xu and Guo 2003; Chen and Cai
 158 2004; Snæbjörnsson et al. 2007; Sterling et al. 2010). The high-sided truck is
 159 modelled as a multibody system composed by individual rigid bodies (the vehicle
 160 body and two rigid bodies for each axle set). The vehicle body connects to
 161 the axle sets by means of the suspension system, which is modelled by linear

162 spring-dashpot elements. The tires are considered as the linear spring-dashpot
 163 elements, in which the bottom node has a contact with the bridge surface. The
 164 vehicle body has five degrees of freedom (DOFs): vertical displacement z_c , lateral
 165 displacement y_c , rolling motion θ_x^c , pitching motion θ_y^c and yawing motion θ_z^c .
 166 Each rigid body in either the front axle set or rear axle set is assigned two DOFs:
 167 vertical displacement z_{ij} and lateral displacement $y_{i,j}$ (where $i = r, f$ is the index
 168 for rear and front axle, respectively and $j = 1, 2$ distinguish the right and left
 169 wheels respect to the driver). A constraint is applied to the two rigid bodies
 170 of each axle set in order to put a rigid connection between them. Altogether,
 171 the vehicle model has 11 DOFs. The geometry and mechanical properties of the
 172 high-sided vehicle are listed in Appendix I.

173 Only one vehicle is considered to be crossing the bridge in each analysis. The
 174 presence of multiple vehicles in the deck is a more realistic traffic scenario. How-
 175 ever, previous research works have observed that the vibration induced by other
 176 vehicles does not change significantly the contact forces of individual vehicles
 177 ([Zhou and Chen 2015](#)).

178 **TURBULENT CROSSWIND GENERATION**

179 The turbulent crosswind is characterized by its stochastic properties: turbu-
 180 lence intensity, integral length scale, power spectral density function and coher-
 181 ence function. For a certain point at height z in space, the wind speed $U(x, y, z, t)$
 182 is composed of three components:

$$U(x, y, z, t) = \begin{pmatrix} U + u(t) \\ v(t) \\ w(t) \end{pmatrix} \quad (3)$$

183 where U is the mean wind speed and $u(t)$, $v(t)$, $w(t)$ are the fluctuating compo-

184 nents of the wind in the longitudinal, lateral and vertical directions, respectively.
 185 The mean wind speed depends on the height z , the terrain roughness and terrain
 186 orography. The mean speed is adopted by the following expression (CEN 2005b):

$$U = k_r \ln \left(\frac{z}{z_0} \right) c_o(z) U_b \quad (4)$$

187 with k_r the terrain factor, z_0 the roughness length, $c_o(z)$ orography factor taken
 188 as 1.0 and U_b the basic wind speed at 10 m above ground of terrain. The terrain
 189 category II is considered for this study, therefore, the value of k_r and z_0 are 0.19
 190 and 0.05 m, respectively. It is noted that expression (4) ignores possible funnelling
 191 effects induced by the narrow shape of the valley where the considered bridge is
 192 located. This is deemed acceptable since the scope of the paper is to apply a
 193 FE-based wind-vehicle-bridge interaction model to a slender arch bridge, without
 194 losing generality in the results by adopting a wind-profile that is particular to an
 195 specific emplacement.

196 The generation of the turbulent wind speed time-histories in different points
 197 in space is carried out by applying the method proposed by Veers (Veers 1988),
 198 considering that these time-histories of wind speed are different but are not in-
 199 dependent. In order to apply the aerodynamic forces of turbulent wind on the
 200 bridge and vehicle, the time histories of turbulent wind components in 53 points
 201 (see Fig. 4) are generated. For this generation of time histories, the value of
 202 the basic wind speed U_b is firstly proposed, and the mean wind speed at each
 203 point are then calculated according to its height. The main data of simulating
 204 conditions are adopted as follows:

- 205 • Integral length scale: $L_u = 100$ m, $L_v = 0.25L_u$ and $L_w = 0.10L_u$ (Strømmen
 206 2006)
- 207 • Turbulent intensities: $I_u(z) = 1/\ln(z/z_0)$, $I_v = 0.75I_u$ and $I_w = 0.50I_u$

208 (Strømmen 2006)

- 209 • Upper cutoff frequency: $f_{up} = 12.0$ Hz
- 210 • Dividing number of frequency: $N_f = 1024$
- 211 • Time interval: $dt = 0.002$ s

212 A range of the basic wind velocity from 5.0 to 30.0 m/s in increments of
213 0.5 m/s has been considered to study the influence of the crosswind velocity,
214 Figure 4(b) shows the time histories of the longitudinal component of turbulent
215 crosswind velocity at the two points indicated in figure 4(a) for $U_b = 10.0$ m/s.

216 WIND-VEHICLE-BRIDGE INTERACTION

217 The coupled vehicle-bridge system under turbulent crosswind is governed by
218 a complicated dynamic interaction problem that involves interaction between the
219 wind and the vehicle, the wind and the bridge, and the vehicle and the bridge.
220 The interaction wind-vehicle and wind-bridge interaction is modelled through the
221 aerodynamic forces applied to the vehicle and the bridge. A detailed description
222 on how to obtain these aerodynamic forces is given in the next section. On the
223 other hand, the vehicle-bridge interaction is established between the tires and
224 the deck surface. In this study, a perfectly guided path is considered for the
225 tire-deck surface interaction model, i.e. contact points between the tires and the
226 deck surface share the position and velocity. In order to develop this tire-deck
227 interaction model in Abaqus, a “node to surface” contact formulation (SIMULIA
228 2011) is used between the bottom node of the tire elements and the deck surface.
229 The augmented Lagrange method is applied then for the kinematic relations
230 to enforce the corresponding contact constraints. Using augmented Lagrange
231 formulation, the force vector applied on the vehicle and the bridge systems due
232 to the interaction can be determined as:

$$\begin{Bmatrix} \mathbf{F}_v^C \\ \mathbf{F}_b^C \end{Bmatrix} = \nabla \Phi^T \mathbf{\Lambda} + \nabla \Phi^T \Upsilon \Phi \quad (5)$$

where $\nabla \Phi^T = \partial \Phi / \partial \mathbf{x}$; $\mathbf{x} = [\mathbf{x}^v, \mathbf{x}^b]$ is the global vector of displacement unknowns, Φ is the constraints vector that links the bottom node of the tire elements with the deck surface; $\mathbf{\Lambda}$ and Υ are the Lagrange multiplier vector and the penalty matrix of the coupled system, respectively; \mathbf{F}_v^c is force vector applied on the vehicle as consequence of the interaction with structure, and \mathbf{F}_b^C their counterparts on the structure.

The proposed methodology is developed in Abaqus (SIMULIA 2011), which allows to model the bridge structure by means of finite elements and the vehicle using multibody systems. The multibody dynamic equilibrium equations include second order and nonlinear terms related to the inertial forces (gyroscopic, coriolis, centrifugal) that, in addition to the inherent nonlinearity introduced by the moving contact in the wheels, leads to a nonlinear coupled system of equations that defines the wind-vehicle-bridge interaction problem. This system can be expressed in the following matrix form, including the interaction forces and aerodynamic forces:

$$\begin{bmatrix} \mathbf{M}_v & \mathbf{0} \\ \mathbf{0} & \mathbf{M}_b \end{bmatrix} \begin{Bmatrix} \ddot{\mathbf{x}}_v \\ \ddot{\mathbf{x}}_b \end{Bmatrix} + \begin{bmatrix} \mathbf{C}_v & \mathbf{0} \\ \mathbf{0} & \mathbf{C}_b \end{bmatrix} \begin{Bmatrix} \dot{\mathbf{x}}_v \\ \dot{\mathbf{x}}_b \end{Bmatrix} + \begin{bmatrix} \mathbf{K}_v & \mathbf{0} \\ \mathbf{0} & \mathbf{K}_b \end{bmatrix} \begin{Bmatrix} \mathbf{x}_v \\ \mathbf{x}_b \end{Bmatrix} = \begin{Bmatrix} \mathbf{F}_v^w \\ \mathbf{F}_b^w \end{Bmatrix} + \begin{Bmatrix} \mathbf{F}_v^C \\ \mathbf{F}_b^C \end{Bmatrix} \quad (6)$$

where \mathbf{F}_v^w , \mathbf{F}_b^w is the aerodynamic wind force vector applied on the vehicle and bridge, respectively; \mathbf{M}_v , \mathbf{C}_v , \mathbf{K}_v are the mass, damping and stiffness matrix of the vehicle, respectively; \mathbf{M}_b , \mathbf{C}_b , \mathbf{K}_b are the mass, damping and stiffness matrix of the bridge, respectively.

252 The HHT- α implicit integration method (Hilber et al. 1977) is used to solve
 253 the system of differential equations (6) in the time domain. A constant time step
 254 of 0.001 s is adopted, which is small enough to accurately capture high frequency
 255 vibrations and to account for the contribution of high-order spatial frequencies
 256 of the roughness profile.

257 **WIND-INDUCED EFFECTS**

258 **Wind forces on the vehicle**

259 The aerodynamics forces and moments acting on the running vehicle under
 260 crosswind are represented in Fig. 5. These are determined using the quasi-static
 261 approach according to (Snæbjörnsson et al. 2007). Assuming that the mean
 262 wind velocity U is perpendicular to the longitudinal axis of the bridge deck (the
 263 x axis) and the vehicle runs over the bridge with a constant speed V the relative
 264 wind velocity U_R and the angle of incidence α (see Fig. 5) can be determined at
 265 each instant t as follows:

$$U_R(t) = \sqrt{(U + u(t))^2 + (v(t) + V)^2} \quad (7)$$

$$\alpha(t) = \arctan \left(\frac{U + u(t)}{v(t) + V} \right) \quad (8)$$

266 where $u(t)$ and $v(t)$ are the longitudinal and horizontal components of turbulent
 267 crosswind, respectively. It should be noted that the wind time-history applied on
 268 the running vehicle is different from that applied on the surrounding nodes of the
 269 deck, from which it is linearly interpolated maintaining the compatibility.

270 **Wind forces on the bridge**

271 Based on the buffeting theory, the wind induced forces on the bridge structure
 272 can be determined from the instantaneous velocity pressure and the loads coeffi-

273 cients. The wind-induced forces per unit length on the bridge may be expressed
 274 in vector form as follows (Strømmen 2006):

$$\begin{bmatrix} F_D(x, t) \\ F_L(x, t) \\ M_x(x, t) \end{bmatrix} = \frac{1}{2} \rho U_R^2 \begin{bmatrix} DC_D(\alpha_e) \\ BC_L(\alpha_e) \\ B^2 C_M(\alpha_e) \end{bmatrix} \quad (9)$$

275 where U_R is the instantaneous relative wind velocity, $C_D(\alpha_e)$, $C_L(\alpha_e)$, $C_M(\alpha_e)$
 276 are drag, lift and moment aerodynamic coefficients that are functions of the angle
 277 of wind incidence α_e (see Fig. 6), D and B are height and width of deck bridge
 278 section. In structural axis, the equation (9) is transformed into:

$$\mathbf{F}_b^w(x, t) = \begin{bmatrix} F_y \\ F_z \\ M_x \end{bmatrix} = \begin{bmatrix} \cos \beta & -\sin \beta & 0 \\ \sin \beta & \cos \beta & 0 \\ 0 & 0 & 1 \end{bmatrix} \begin{bmatrix} F_D \\ F_L \\ M_x \end{bmatrix} \quad (10)$$

279 The formulation using the Scanlan's frequency dependent flutter derivatives
 280 (Scanlan and Tomko 1971) is usually used in the modal frequency domain. How-
 281 ever, in this study the dynamic calculation is performed in the direct time domain,
 282 therefore, the aerodynamic forces can be decomposed, using the linearization ap-
 283 proach, as follows (Strømmen 2006):

$$\mathbf{F}_b^w = \underbrace{\mathbf{F}_s}_{\text{static}} + \underbrace{\mathbf{B} \cdot \mathbf{v}}_{\text{aerodynamic}} + \underbrace{\mathbf{C}_{ae} \cdot \dot{\mathbf{r}} + \mathbf{K}_{ae} \cdot \mathbf{r}}_{\text{aeroelastic}} \quad (11)$$

284 where \mathbf{F}_s , $\mathbf{B} \cdot \mathbf{v}$ and $\mathbf{C}_{ae} \cdot \dot{\mathbf{r}} + \mathbf{K}_{ae} \cdot \mathbf{r}$ represent the static, aerodynamic and aeroelastic

285 effects, respectively, and are defined as:

$$\mathbf{F}_s = \frac{1}{2}\rho U^2 B \begin{bmatrix} (D/B)C_D \\ C_L \\ BC_M \end{bmatrix} \bigg|_{\alpha_s} \quad (12a)$$

$$\mathbf{B} = \frac{1}{2}\rho UB \begin{bmatrix} 2(D/B)C_D & (D/B)C'_D - C_L \\ 2C_L & C'_L + (D/B)C_D \\ 2BC_M & BC'_M \end{bmatrix} \bigg|_{\alpha_s} \quad (12b)$$

$$\mathbf{C}_{ae} = -\frac{1}{2}\rho UB \begin{bmatrix} 2(D/B)C_D & (D/B)C'_D - C_L & 0 \\ 2C_L & C'_L + (D/B)C_D & 0 \\ 2BC_M & BC'_M & 0 \end{bmatrix} \bigg|_{\alpha_s} \quad (12c)$$

$$\mathbf{K}_{ae} = \frac{1}{2}\rho U^2 B \begin{bmatrix} 0 & 0 & (D/B)C'_D \\ 0 & 0 & C'_l \\ 0 & 0 & BC'_M \end{bmatrix} \bigg|_{\alpha_s} \quad (12d)$$

$$\mathbf{v} = \begin{bmatrix} u & w \end{bmatrix}^T \quad (12e)$$

$$\mathbf{r} = \begin{bmatrix} p & h & \alpha \end{bmatrix}^T \quad (12f)$$

286 in which α_s is the angle of attack of the wind respect to the position of the bridge
 287 elements (deck, arch, piers) at the static equilibrium position. p , h , α are the
 288 horizontal, vertical and torsional displacement of the structure under turbulent
 289 wind (see Fig. 6). The prime symbol in C'_D , C'_L , C'_M indicates derivation of the
 290 aerodynamic coefficients with respect to the angle of attack. These derivatives
 291 are obtained from the computational fluid dynamic analysis of the deck, arch
 292 and piers (see Appendix III). It can be seen that the static and aerodynamic
 293 parts are functions of the mean wind (U) and its turbulence (u and w), while

294 the aeroelastic part is associated with the structural velocity and displacement.
 295 The static and aerodynamic parts can be introduced into the structural elements
 296 via nodal forces in Abaqus software. However, due to the structural motion
 297 dependence of the aeroelastic part there is no direct way to introduce these forces
 298 in Abaqus software. In order to model the aeroelastic wind forces an user element
 299 has been developed within Abaqus using user subroutine UEL ([SIMULIA 2011](#)).
 300 The basic idea used here is that the user element is attached to each node of the
 301 structural bridge element as shown in Fig. 7. The user element will provide to
 302 the model during the transient analysis steps the forces \mathbf{F}_i at the node i that
 303 depend on the values of the degrees of freedom \mathbf{X}_i^b at this node (each structural
 304 bridge element has six degrees of freedom).

305 It is noted that the forces \mathbf{F}_i generated by user element must be the same
 306 aeroelastic wind forces acting on this node, therefore, the nodal forces \mathbf{F}_i can be
 307 expressed as

$$\mathbf{F}_i = \mathbf{C}_i^{ae} \dot{\mathbf{X}}_i^b + \mathbf{K}_i^{ae} \mathbf{X}_i^b \quad (13)$$

308 where \mathbf{K}_i^{ae} and \mathbf{C}_i^{ae} represent the local aeroelastic stiffness and damping matrices
 309 at the node i , respectively. From the equations (12d) and (12e), the expressions

of \mathbf{K}_i^{ae} and \mathbf{C}_i^{ae} can be determined as following

$$\mathbf{K}_i^{ae} = \frac{1}{2}\rho U^2 B l_{wi} \begin{bmatrix} 0 & 0 & 0 & 0 & 0 & 0 \\ 0 & 0 & 0 & (D/B)C'_D & 0 & 0 \\ 0 & 0 & 0 & C'_L & 0 & 0 \\ 0 & 0 & 0 & BC'_M & 0 & 0 \\ 0 & 0 & 0 & 0 & 0 & 0 \\ 0 & 0 & 0 & 0 & 0 & 0 \end{bmatrix} \bigg|_{\alpha_s} \quad (14a)$$

$$\mathbf{C}_i^{ae} = -\frac{1}{2}\rho U B l_{wi} \begin{bmatrix} 0 & 0 & 0 & 0 & 0 & 0 \\ 0 & 2(D/B)C_D & (D/B)C'D - C_L & 0 & 0 & 0 \\ 0 & 2C_L & C'_L + (D/B)C_D & 0 & 0 & 0 \\ 0 & 2BC_M & BC'_M & 0 & 0 & 0 \\ 0 & 0 & 0 & 0 & 0 & 0 \\ 0 & 0 & 0 & 0 & 0 & 0 \end{bmatrix} \bigg|_{\alpha_s} \quad (14b)$$

where l_{wi} is the length along which the wind forces acting on the structural element are lumped to the node i . The above definition of the UEL is presented with generality and it is readily applicable to any FE software. Further details on the specified implementation of this UEL to Abaqus are described in Appendix II. Using this methodology, the wind induced forces are applied to all the bridge elements, including the deck, the arch and the piers.

RESULTS AND DISCUSSION

The deck of the Wild bridge has been designed to support two road lanes and one sidewalk as shown in Fig. 8. With this design, the road axis is eccentric 0.35 m with respect to the bridge axis which implies that the vehicles run over the bridge with certain eccentricity. In the previous work (Nguyen et al. 2015),

322 it's observed that the larger the vibration at the sidewalk is obtained when the
323 passing vehicle is transversely closer to the sidewalk. Therefore, the load case in
324 which the vehicle runs on the lane 1 with eccentricity of 1.4 m is selected for this
325 study (see Fig. 8). To eliminate the possible effect generated due to the suddenly
326 applied aerodynamic wind forces on the dynamic response of the vehicle and to
327 study the possible effect generated during the time that the vehicle enters and
328 leaves the bridge, the external platforms with roughness surface are considered
329 at both abutments of the bridge in all calculations.

330 As mentioned in section 4, in order to study the influence of the crosswind
331 different levels of the basic wind velocity are used. In fact, a range from 5.0 to
332 30.0 m/s in increment of 0.5 m/s has been considered. Furthermore, for each
333 level of basic wind velocity, a range of vehicle velocities ranging from 60 to 120
334 km/h, in increments of 10 km/h, is considered to investigate the ride comfort and
335 safety of the road vehicle. An extensive number of analyses are performed and
336 the main obtained results are presented and discussed below.

337 **Effects of crosswind on the bridge vibration**

338 In order to assess effects of the turbulent crosswind on the bridge vibration, the
339 time histories of vertical and lateral acceleration of all points along the sidewalk
340 are recorded in all calculations. The maximum acceleration at each point is then
341 determined. Fig. 9(a) shows the peak vertical acceleration along the sidewalk
342 for different levels of the basic wind velocity when the vehicle crosses the bridge
343 at $v = 100$ km/h. The result without crosswind is also included for comparison.
344 It can be observed that for gentle crosswind ($U_b = 5$ m/s) the vibration of deck
345 is similar to the case without crosswind. It can be due to that the aerodynamic
346 wind forces are too low to produce any meaningful inertia effects, comparing with
347 the forces generated by the passing vehicle. But, as the crosswind is stronger and

348 more moderate, the vibration of deck is larger. Furthermore, it is seen that the
 349 zone of arch span is the one more affected by the crosswind as expected, since
 350 the wind velocity in this zone is higher. In fact, if the basic wind velocity is of
 351 25.0 m/s, the maximum vertical acceleration obtained at point C₁ can be up to
 352 10.5 times higher than the case without crosswind and 1.5 times higher than the
 353 maximum acceleration allowed ($a_{lim} = 0.5\sqrt{f_0} = 0.81 \text{ m/s}^2$) by some codes (BS
 354 5400-2:2006 2006; RPX-95 1995) for deck vibration. Moreover, from Fig. 9(a)
 355 the impact effect can be observed when the vehicle enters and leaves the bridge.
 356 Such peak acceleration at the deck nearby the abutments would far exceed the
 357 admissible limit in SLS of vibration (a_{lim}). The human response to vibration
 358 depends, of course, on the level or magnitude of vibration, but also depends on
 359 the other important factors such as frequency content of the vibration, exposure
 360 time, direction of application, etc. Further analysis have been done in order to
 361 evaluate the human comfort. The RMS acceleration in one-third octave frequency
 362 bands are obtained from the acceleration time histories. These RMS acceleration
 363 are then compared with the vertical base curve for acceptable human response
 364 under storm conditions proposed by Irwin (Irwin 1978). A representative result
 365 is shown in Fig. 9(b), in which the vertical RMS accelerations at the point C₁
 366 are represented for different levels of the basic wind velocity. The result in Fig.
 367 9(b) reaffirms the important influence of crosswind on the vertical vibration of
 368 this bridge and the need for considering the aerodynamic actions introduced by
 369 wind in the general vibration assessment of bridges. Additionally, it can be seen
 370 that the RMS accelerations will exceed the limit comfort curve considering the
 371 threshold for frequent events when the wind is strong (25.0 m/s), which means
 372 that the human, in this case, pedestrian users feel or sense discomfort due to the
 373 bridge vibration.

374 Respect to the lateral vibration of the bridge, the same results are represented

375 in Fig. 10. The peak lateral accelerations along the sidewalk are obtained and
 376 plotted for different levels of the basic wind velocity (U_b), and compared with
 377 the limit of comfort established by IAP-11 (IAP-11 2011) ($a_{lim} = 0.8 \text{ m/s}^2$) (see
 378 Fig. 10(a)). The RMS accelerations in one-third octave frequency bands at
 379 the point C_1 are also plotted and compared with the lateral acceleration base
 380 curve for acceptable human response proposed by Irwin (Irwin 1978). Figure
 381 10(a) shows that the peak lateral acceleration on the deck is only increased by
 382 the crosswind on the sections corresponding to the arch due to the increased
 383 transverse flexibility of the bridge in this area. Furthermore, this effect is only
 384 appreciable for relatively strong wind speeds, which is attributed to important
 385 slenderness of the deck and the reduced aerodynamic forces. However, from Fig.
 386 10(b) it can be noted that the crosswind has an important effect on the frequency
 387 content of the acceleration signals of this structure, specially in the range $[0.4-10]$
 388 Hz. The RMS acceleration in one-third octave bands at point C_1 increases with
 389 the wind velocity, and it nearly reaches the limit curve for $U_b = 25.0 \text{ m/s}$. This
 390 demonstrates that, as expected, the pedestrians comfort decreased by increasing
 391 the lateral wind speed and it can only be tackled by using criteria that account
 392 for the excitation frequency, such as Irwin's

393 In order to explore the participation of the wind- and traffic-induced vibration
 394 on the frequency content of the response of the deck, the time histories of the deck
 395 acceleration is analyzed in the frequency domain. Fig. 11 shows the frequency
 396 content of the vertical and lateral acceleration at point C_1 when the vehicle crosses
 397 over the bridge at $V = 100 \text{ km/h}$, for different basic wind speeds. It can be
 398 observed from Fig. 11(a) that three modes dominate the vertical deck vibration.
 399 The dominance of the first vertical mode is observed, specially for strong winds
 400 ($U_b = 25.0 \text{ m/s}$), but it is also apparent the important participation of the third
 401 vertical mode (approximately 5 Hz) and the torsional mode (in the range of 10

Hz). This result directly questions the applicability of extended comfort criteria that are based on the assumption that the structure is completely dominated by a fundamental mode of vibration (BS 5400-2:2006 2006; RPX-95 1995). In comparison to the vertical vibration of the deck, the lateral vibration (Fig. 11(b)) is more dominated by the first lateral mode for wind velocities below 20 m/s, beyond this value a group of closely spaced high-order mode between 5 and 10 Hz increases significantly the response as shown in Fig. 11(b).

Effects of crosswind on the road vehicle vibration

In this section, the ride comfort and safety of road vehicle are addressed through the accelerations at the driver seat (see Fig. 3), the contact forces between the tire and road. The weighted RMS acceleration and the RMS acceleration in one-third octave frequency bands are obtained from the time histories of the vertical and lateral acceleration at the driver's seat in order to evaluate the vehicle users' comfort. The resulting accelerations are compared with the indicative ranges of comfort given by ISO 2631 (ISO 2631-1:1997 1997) and fatigue-decreased proficiency boundaries proposed by ISO 2631 (ISO 2631:1978 1978), respectively. Figure 12 shows the results for the vertical vibration of the vehicle. It can be observed that the maximum acceleration at driver's seat is hardly affected by crosswinds below ranging from 5 to 20 m/s (see Fig. 12(a)), which is also noticed for the the weighted RMS accelerations (see Fig. 12(b)). Furthermore, there are high increments of acceleration for strong wind ($U_b = 25.0$ m/s) compared with the other lower wind velocities. This is due to the fact that the strong wind increases the vehicle vibration on the one hand, and increases the bridge vibration on the other which also influences the vehicle vibration, as shown in Fig. 14(a). Interestingly, all recorded values of RMS accelerations in the vehicle are regarded as "uncomfortable" according to ISO's criterion (ISO

2631-1:1997 1997), including the case in which the wind is not considered and for all the vehicle velocities considered. The validity of the comfort criteria for the vertical vibrations in the vehicle considered should be questioned based on these results. Firstly, it is noted that the scope of this work is the global assessment of the user's comfort and safety due to the wind-vehicle-bridge interaction, and no attempt was made to simulate the filtering effect of the vehicle seat or other local effects in the vehicle. Secondly, the indicative comfort range proposed by ISO 2631 (ISO 2631-1:1997 1997) gives approximate indications of likely reactions to various magnitudes of overall vibration total values in public transport, and ISO 2631 does not define any limit for acceptable values of magnitude for comfort. From Fig. 12(c) and 12(d), it can be seen that the crosswind hardly effect on the vertical ride comfort of vehicle.

Fig. 13 shows the results of the lateral vibration of vehicle. It is observed that the crosswind influences significantly the lateral acceleration in the vehicle and the comfort of its user regarding vibrations in this direction. Indeed, the peak acceleration and the weighted RMS acceleration increase by increasing the crosswind velocity. The RMS accelerations in the one-third octave bands are also larger when the crosswind speed increases. The RMS accelerations almost reach the limit curve for fatigue-decreased proficiency when the velocity of the vehicle is 120 km/h and the crosswind speed is 25.0 m/s, indicating that the driver could feel fatigue and decrease his proficiency to drive. In contrast to the vertical vibration of the vehicle, its lateral vibration is not influenced by the bridge vibration, but is only influenced by its lateral vibration modes, as shown in Fig. 14(b).

Vehicle accidents can be categorized in three main types: overturning, side-slipping and yawing (rotational) accidents (Baker and Reynolds 1992). Side-slipping accidents and yawing may occur if the coefficient of friction between the

tires and the road surface is low (Snæbjörnsson et al. 2007; Zhou and Chen 2015) (e.g. in wet pavements). However, the assessment of side-slipping and, especially, yawing accidents, requires detailed information about the contact between the tires and the pavement, as well as the model of the driver’s response (Chen and Cai 2004). This work will focus only on vehicle overturnings because it represents the most common type of wind-induced vehicle accidents (Baker and Reynolds 1992). It should be noted, however, that the methodology presented in this paper is applicable to the study of the other types of accidents.

An overturning accident occurs when one of the tire reactions is zero, in other words, the vertical load is transferred from the tires on the windward side of the vehicle to those on the leeward side. The Load Transfer Ratio (LTR) is employed to quantify the load transference and is defined as:

$$LTR = \frac{F_L - F_R}{F_L + F_R} \quad (15)$$

where F_L and F_R are the vertical tire reactions on the left (leeward) and right (windward) sides, respectively. The LTR is 0.0 when the loads on two sides are equal and ± 1.0 when all the load is transferred to the leeward side and the vehicle is on the verge of an overturning accident. The LTR of the front and rear wheels are plotted in Fig. 15(a) for a certain vehicle and wind velocity. It can be observed that the load transfer reaches larger value when the vehicle is at the arch span, as expected. This is because that the crosswind velocity in this section of the bridge is higher than those of other sections of the bridge. The LTR at the rear wheel is higher than at the front wheel, as expected. It is due to that the rear wheels have less gravity load from the carbody by the position of gravity centre, and therefore these wheels govern the overturning accident.

Based on the LTR, the critical wind speed can be determined for each vehicle

479 velocity when at this speed the vehicle overturns. Consequently, the critical wind
480 curve (CWC) can be obtained from the all critical wind speed for the whole range
481 of the vehicle velocities. Figure 15(b) represents the CWC obtained in this work
482 for the bridge. Assuming a vehicle velocity limit of 120 km/h, it is observed that
483 no restriction should be imposed when the wind speed is below 15 m/s, which
484 could be considered as the critical wind speed for this bridge.

485 CONCLUSIONS

486 In this paper, the dynamic effects of turbulent crosswind on the serviceability
487 state of vibrations and the vehicle accident risk are addressed in a slender arch
488 by means of the wind-vehicle-bridge interaction analyses. A new finite element is
489 developed for the application of aerodynamic wind actions in general Finite Ele-
490 ment Analysis software packages. This element is able to provide the aeroelastic
491 wind forces. The results of the fully coupled nonlinear dynamic analysis drawn
492 the following conclusions on the dynamic response of the studied bridge:

- 493 • The bridge vibration is significantly affected by the crosswind in terms
494 of the peak acceleration and the frequency content when the crosswind is
495 moderate and strong ($U_b > 15$ m/s). However, for lower wind speeds (below
496 10 m/s) the deck vibration is governed by the passing vehicle.
- 497 • The criteria for the SLS of vertical vibration based on the peak acceleration
498 is easily exceeded at almost point of the deck when the crosswind is strong
499 ($U_b = 25.0$ m/s). Analyzing in the frequency domain the vibration level is
500 still below the limit comfort curve, and therefore, is comfortable. Further-
501 more, the vertical bridge vibration is significantly influenced by high-order
502 vibration modes between 5 and 10 Hz that would be ignored according to
503 code-based comfort criteria such as ([BS 5400-2:2006 2006](#); [RPX-95 1995](#)).

- 504 • Previous research works observed the importance of the road roughness
505 surface on the ride comfort of the vehicle. In this study, it is observed that it
506 also depends on the vehicle velocity and the crosswind speed. It is observed
507 that the crosswind has more effect on ride comfort of the vehicle in lateral
508 direction than in the vertical direction. When the vehicle runs over the
509 bridge with the velocity of 120 km/s and with a strong crosswind velocity
510 ($U_b = 25.0$ m/s), the driver could experience the fatigue and decrease his
511 proficiency to drive.
- 512 • For the “good” road surface quality considered in this study, the basic wind
513 speed of 15 m/s could be considered as the critical speed in the studied
514 bridge for the circulation.

515 **ACKNOWLEDGEMENTS**

516 The authors thank to other members of the team of Intitut für Betonbau at
517 Technical University of Graz: Bernhard Freytag, Michael Reichel, who provided
518 the necessary information of the Wild bridge design. K.Nguyen and O. Rio also
519 thank to the MINECO of Spain for the support of the project BIA2013-48480-
520 C2-1R.

521 **REFERENCES**

- 522 American Association of State Highway and Transportation Officials (1998).
523 *AASHTO LRFD: Bridge design specifications*. Washington, EE UU.
- 524 Azizinamini, A., Barth, K., Dexter, R., and Rubeiz, C. (2004). “High Performance
525 Steel: Research FrontHistorical Account of Research Activities.” *Journal of*
526 *Bridge Engineering*, 9(3), 212–217.
- 527 Baker, C. J. and Reynolds, S. (1992). “Wind-induced accidents of road vehicles.”
528 *Accident Analysis and Prevention*, 24(6), 559–575.

529 Boggs, D. and Petersen, C. P. (1995). “Acceleration indexes for human comfort
530 in tall buildings - peak or rms?”

531 BS 5400-2:2006 (2006). *Steel, concrete and composite bridges - Part 2: Specification
532 for loads*. British Standard, UK.

533 BS 6841:1987 (2012). *Guide to measurement and evaluation of human exposure
534 to whole-body mechanical vibration and repeated shock*.

535 Cai, C. and Chen, S. (2004). “Framework of vehiclebridgewind dynamic analysis.”
536 *Journal of Wind Engineering and Industrial Aerodynamics*, 92(7-8), 579–607.

537 Camara, A., Nguyen, K., Ruiz-Teran, A., and Stafford, P. (2014). “Serviceabil-
538 ity limit state of vibrations in under-deck cable-stayed bridges accounting for
539 vehicle-structure interaction.” *Engineering Structures*, 61, 61–72.

540 CEN (2005a). *EN 1337-3:2005 Structural bearings. Part 3: Elastomeric bearings*.
541 rue de Stassart, 36B-1050 Brussels.

542 CEN (2005b). *EN 1991-1-4: Actions on structures - Part 1-4: General actions -
543 Wind actions*. rue de Stassart, 36B-1050 Brussels.

544 Chen, S. R. and Cai, C. S. (2004). “Accident assessment of vehicles on long-span
545 bridges in windy environments.” *Journal of Wind Engineering and Industrial
546 Aerodynamics*, 92(12), 991–1024.

547 Chen, X., Matsumoto, M., and Kareem, A. (2000). “Time Domain Flutter and
548 Buffeting Response Analysis of Bridges.” *Journal of Engineering Mechanics*,
549 126(1), 7–16.

550 Davenport, A. (1962). “Buffeting of a Suspension Bridge by Storm Winds.” *Jour-
551 nal of the Structural Division*, 88(3), 233–270.

552 Dodds, C. and Robson, J. (1973). “The description of road surface roughness.”
553 *Journal of Sound and Vibration*, 31(2), 175–183.

554 Griffin, M. J. (1990). *Handbook of Human Vibration*. Academic Press Inc. (Lon-
555 don) Limited.

556 Guo, W. H. and Xu, Y. L. (2006). “Safety Analysis of Moving Road Vehicles on
557 a Long Bridge under Crosswind.” *Journal of Engineering Mechanics*, 132(4),
558 438–446.

559 Hilber, H. M., Hughes, T. J., and Taylor, R. L. (1977). “Improved numerical
560 dissipation for time integration algorithms in structural dynamics.” *Earthquake
561 Engineering and Structural Dynamics*, 5, 283–292.

562 IAP-11 (2011). *IAP-11: Instrucción sobre las acciones a considerar en el proyecto
563 de puentes de carretera (in Spanish)*.

564 Irwin, A. W. (1978). “Human response to dynamic motion of structures.” *The
565 Structural Engineer*, 56A(9), 237–244.

566 ISO 2631-1:1997 (1997). *Mechanical vibration and shock – Evaluation of human
567 exposure to whole-body vibration – Part 1: General requirements*. International
568 Organization for Standardization, Geneva.

569 ISO 2631:1978 (1978). *Guide for the evaluation of human exposure to whole-body
570 vibration*. International Organization for Standardization, Geneva.

571 ISO 8608:1995 (1995). *Mechanical vibration - Road surface profiles - Reporting of
572 measured data*. International Organization for Standardization (ISO), Geneva.

573 JCSS (2001a). *Probabilistic Model Code - Part 2: Load Models*.

574 JCSS (2001b). *Probabilistic Model Code - Part 3: Material Properties*.

575 Kamash, K. M. A. and Robson, J. D. (1978). “The Application of Isotropy in
576 Road Surface Modelling.” *Journal of Sound and Vibration*, 57(1), 89–100.

577 Kühne, M. and Orgass, M. (2009). “Prüfbericht PB 1.1/09-126-4 : Überwachung
578 und Prüfung von UHFRc für das Bauvorhaben, Wild-Brücke.” *Report no.*,
579 MFPA Leipzig GmbH.

580 Miyata, T. and Yamada, H. (1990). “Coupled flutter estimate of a suspension
581 bridge.” *Journal of Wind Engineering and Industrial Aerodynamics*, 33, 341–
582 348.

583 Moghimi, H. and Ronagh, H. R. (2008). “Development of a numerical model
584 for bridgevehicle interaction and human response to traffic-induced vibration.”
585 *Engineering Structures*, 30(12), 3808–3819.

586 Nguyen, K., Freytag, B., Ralbovsky, M., and Rio, O. (2015). “Assessment of
587 serviceability limit state of vibrations in the UHPFRC-Wild bridge through an
588 updated FEM using vehicle-bridge interaction.” *Computers & Structures*, 156,
589 29–41.

590 Roeder, C. W., Barth, K. E., and Bergman, A. (2004). “Effect of Live-Load
591 Deflections on Steel Bridge Performance.” *Journal of Bridge Engineering*, 9(3),
592 259–267.

593 RPX-95 (1995). *RPX-95: Recommendations for the project of composite road*
594 *bridges (in Spanish)*. Spain.

595 Sayers, M. W. (1988). “Dynamic Terrain Inputs to Predict Structural Integrity of
596 Ground Vehicles.” *Report No. UMTRI-88-16*, University of Michigan, Trans-
597 portation Research Institute, Michigan.

598 Scanlan, R. (1978). “The action of flexible bridges under wind, II: Buffeting
599 theory.” *Journal of Sound and Vibration*, 60(2), 201–211.

600 Scanlan, R. and Tomko, A. (1971). “Airfoil and Bridge Deck Flutter Derivatives.”
601 *Journal of the Engineering Mechanics Division*, 97(6), 1717–1737.

602 SIMULIA (2011). *Abaqus Analysis User’s Manual, v6.11*. Dassalt Systemes
603 SIMULIA Corp.

604 Snæbjörnsson, J. T., Baker, C. J., and Sigbjörnsson, R. (2007). “Probabilistic
605 assessment of road vehicle safety in windy environments.” *Journal of Wind*
606 *Engineering and Industrial Aerodynamics*, 95(9-11), 1445–1462.

607 Sparowitz, L., Freytag, B., Reichel, M., and Zimmermann, W. (2011). “Wild
608 Bridge - A Sustainable Arch Made of UHPFRC.” *3rd Chinese - Croatian Joint*
609 *Colloquium: Sustainable Arch Bridges*, Zagreb, Croatia, 45–70.

610 Sterling, M., Quinn, A. D., Hargreaves, D. M., Cheli, F., Sabbioni, E., Tomasini,
 611 G., Delaunay, D., Baker, C. J., and Morvan, H. (2010). “A comparison of
 612 different methods to evaluate the wind induced forces on a high sided lorry.”
 613 *Journal of Wind Engineering and Industrial Aerodynamics*, 98(1), 10–20.
 614 Strømmen, E. (2006). *Theory of Bridge Aerodynamics*. Springer.
 615 Veers, P. S. (1988). “Three-dimensional wind simulation.” *SANDIA report*,
 616 *SAND88-0152 UC-261*, Sandia National Laboratories, California, USA.
 617 Weller, H. G., Tabor, G., Jasak, H., and Fureby, C. (1998). “A tensorial ap-
 618 proach to computational continuum mechanics using object-oriented tech-
 619 niques.” *Computers in Physics*, 12(6), 620–631.
 620 Wright, R. N. and Walker, W. H. (2004). “Criteria for deflection of steel bridges.”
 621 *Bulletin for the America Iron and Steel Institute*, 19.
 622 Xu, Y. and Guo, W. (2004). “Effects of bridge motion and crosswind on ride
 623 comfort of road vehicles.” *Journal of Wind Engineering and Industrial Aero-*
 624 *dynamics*, 92(7-8), 641–662.
 625 Xu, Y. L. and Guo, W. H. (2003). “Dynamic analysis of coupled road vehicle and
 626 cable-stayed bridge systems under turbulent wind.” *Engineering Structures*, 25,
 627 473–486.
 628 Xu, Y. L., Sun, D. K., Ko, J. M., and Lin, J. H. (2000). “Fully coupled buffeting
 629 analysis of Tsing Ma suspension bridge.” *Journal of Wind Engineering and*
 630 *Industrial Aerodynamics*, 85(1), 97–117.
 631 Zhou, Y. and Chen, S. (2015). “Fully coupled driving safety analysis of moving
 632 traffic on long-span bridges subjected to crosswind.” *Journal of Wind Engi-*
 633 *neering and Industrial Aerodynamics*, 143, 1–18.

634 **APPENDIX I. PROPERTIES OF THE HIGH-SIDED TRUCK**

635 The main properties of the high-sided truck are listed in Table III.

636 APPENDIX II. IMPLEMENTATION OF USER ELEMENT

637 The user element is composed by 2 nodes. Each node has six degrees of
 638 freedom. In order to implement this element into the Abaqus software, there
 639 are two essential outputs that are required to be updated in the UEL subroutine
 640 (SIMULIA 2011). In particular, the residual quantity $\mathbf{RHS} := \mathbf{F}$ and the element
 641 Jacobian $\mathbf{AMATRX} := -\partial \mathbf{F} / \partial \mathbf{u}$ must be updated in every interaction. The
 642 program Abaqus uses an implicit time integration and a full Newton solution
 643 technique to solve the static and dynamic problem. In the static analysis, the
 644 user element implemented here does not contribute any stiffness to the model,
 645 while this element will provide the nodal forces to the model in the dynamic
 646 analysis. The nodal forces depend on the values of the degrees of freedom of the
 647 nodes and according to (13) the nodal forces provided by the element is expressed
 648 as

$$\mathbf{G} = \mathbf{C}\dot{\mathbf{u}} + \mathbf{K}\mathbf{u} \quad (16)$$

649 where

$$\mathbf{C} = \begin{bmatrix} \mathbf{C}_i^{ae} & \mathbf{0} \\ \mathbf{0} & \mathbf{C}_i^{ae} \end{bmatrix} \text{ and } \mathbf{K} = \begin{bmatrix} \mathbf{K}_i^{ae} & \mathbf{0} \\ \mathbf{0} & \mathbf{K}_i^{ae} \end{bmatrix} \quad (17)$$

650 According to (SIMULIA 2011), for the integration dynamic analysis the residual
 651 quantity and the element Jacobian at time $t + \Delta t$ must be determined as following

$$\mathbf{RHS} = \mathbf{F} = -\mathbf{M}\ddot{\mathbf{u}}_{t+\Delta t} + (1 + \alpha)\mathbf{G}_{t+\Delta t} - \alpha\mathbf{G}_t \quad (18a)$$

$$\mathbf{AMATRX} = \mathbf{M}(d\ddot{\mathbf{u}}/d\mathbf{u}) + (1 + \alpha)\mathbf{C}(d\dot{\mathbf{u}}/d\mathbf{u}) + (1 + \alpha)\mathbf{K} \quad (18b)$$

652 where \mathbf{M}^{NM} is the mass matrix of the user element (for the implemented element,
653 $\mathbf{M}^{NM} = [\mathbf{0}]$), α is the factor for numerical damping used in HHT method. The
654 values of the nodal forces are recorded as solution-dependent state variables for
655 each time increment in order to determine **RHS** as defined in equation (18a).

656 **APPENDIX III. AERODYNAMIC PROPERTIES OF BRIDGE**

657 The aerodynamic coefficients and their derivatives are obtained from two di-
658 mensional Computational Fluid Dynamic analysis of the deck, arch and pier
659 sections using OpenFOAM v.2.3 ([Weller et al. 1998](#)). The turbulence model fol-
660 lows the Reynolds Average Simulation (RAS) technique. The Reynolds number
661 in the analyses is in the order of 10^7 . Care was taken on the selection of the mesh
662 size. After a sensitivity analysis the element size in the vicinity of the obstacles
663 is selected as 3 mm.

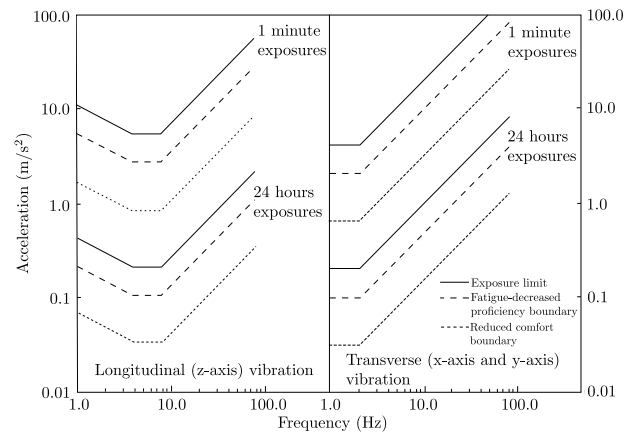
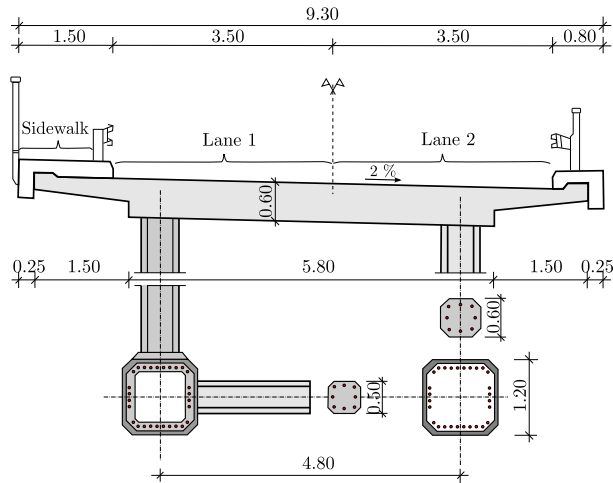


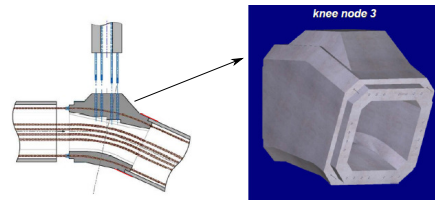
FIG. 1. Exposure limits, fatigue-decreased proficiency boundaries and reduced comfort boundaries to whole-body vibrations given in ISO 2631:1978 (adapted from Handbook of Human Vibration, M. J. Griffin ([Griffin 1990](#)), Chapter 10 “Whole-body Vibration Standards”, 415–451, Copyright 1990, with permission from Elsevier)



(a)



(b)



(c)

FIG. 2. Wild Bridge: (a) general view (image by L. Sparowitz), (b) cross section, (c) knee node

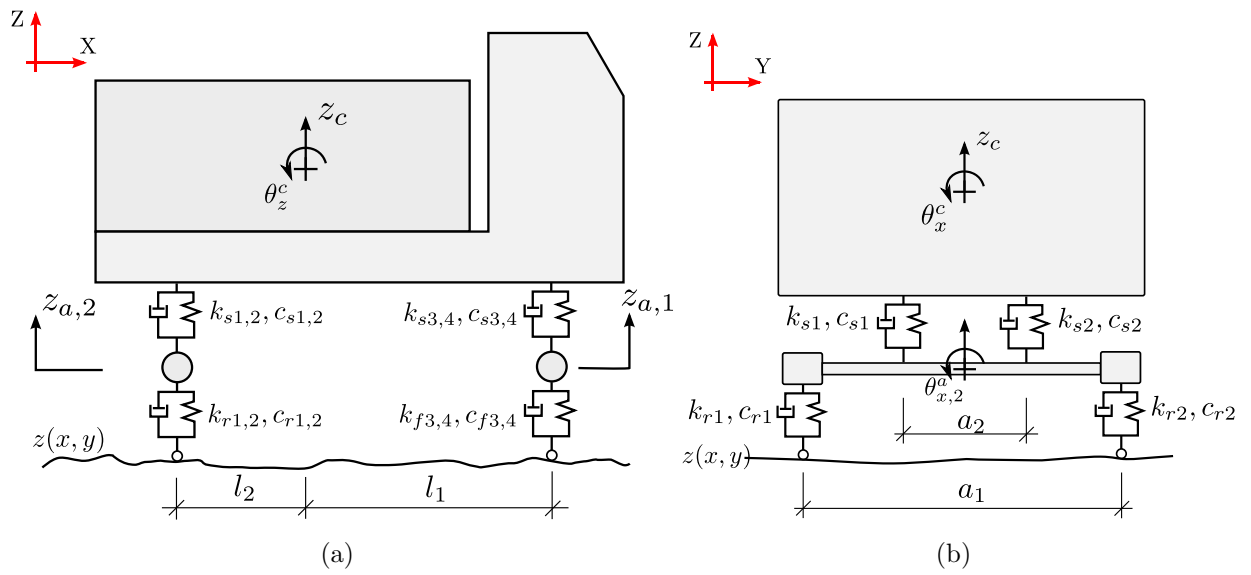
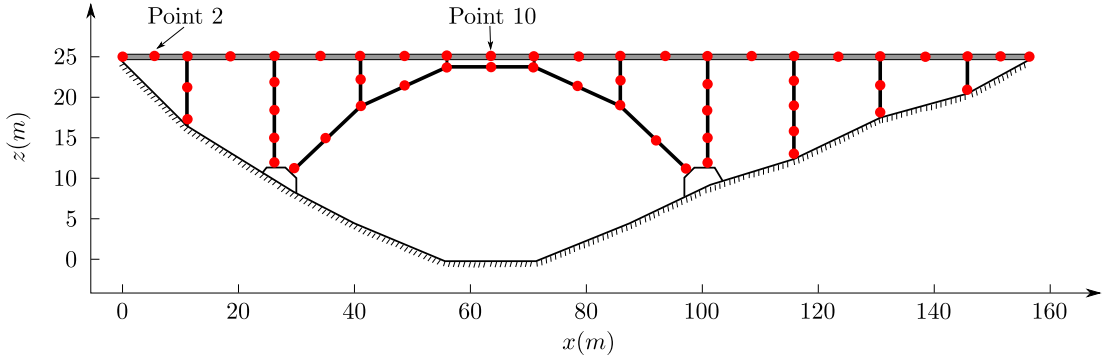
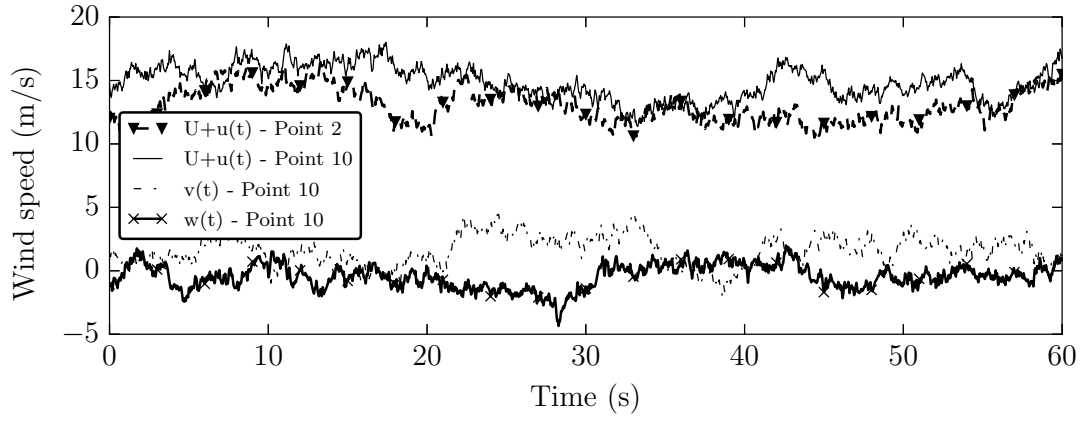


FIG. 3. High-sided vehicle model in dynamic analysis: (a) side view, (b) front view



(a)



(b)

FIG. 4. Simulated wind speed: (a) Position of 53 points for wind speed time histories, (b) Turbulent wind speed at different points for $U_b = 10.0$ m/s

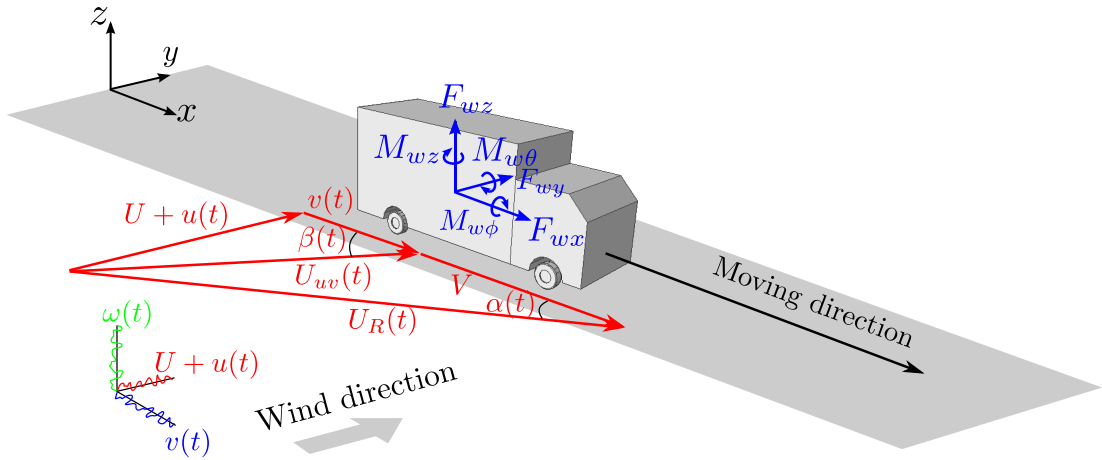


FIG. 5. Relative wind velocity to the running vehicle

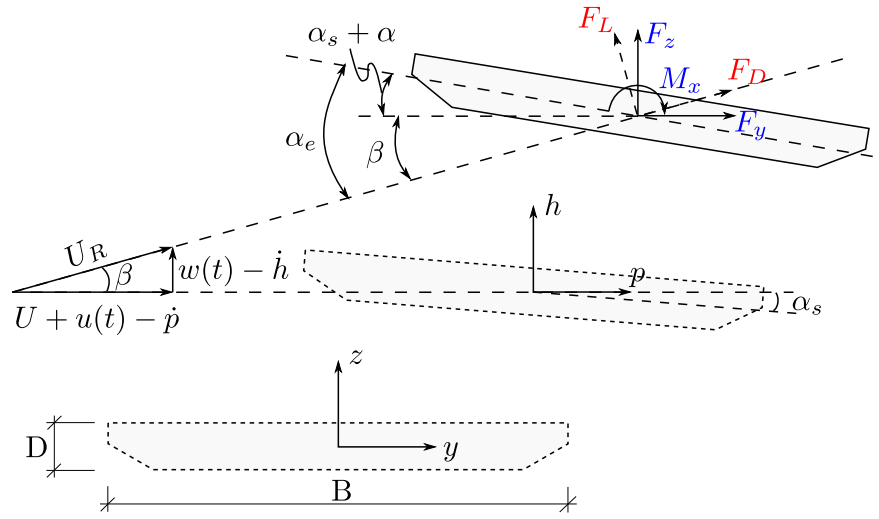


FIG. 6. Diagram of turbulent crosswind acting on bridge elements

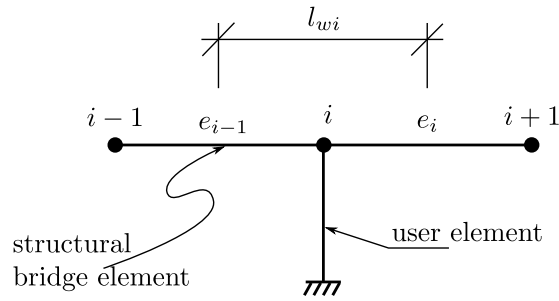


FIG. 7. User element for modelling the aeroelastic wind forces

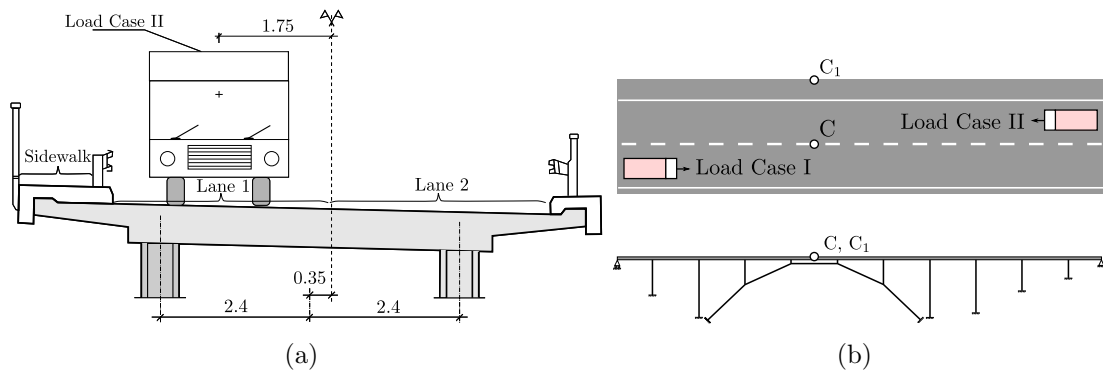


FIG. 8. Load case considered in this study: (a) cross section, (b) plan view and elevation of the bridge, including some control points employed to refer the ongoing results

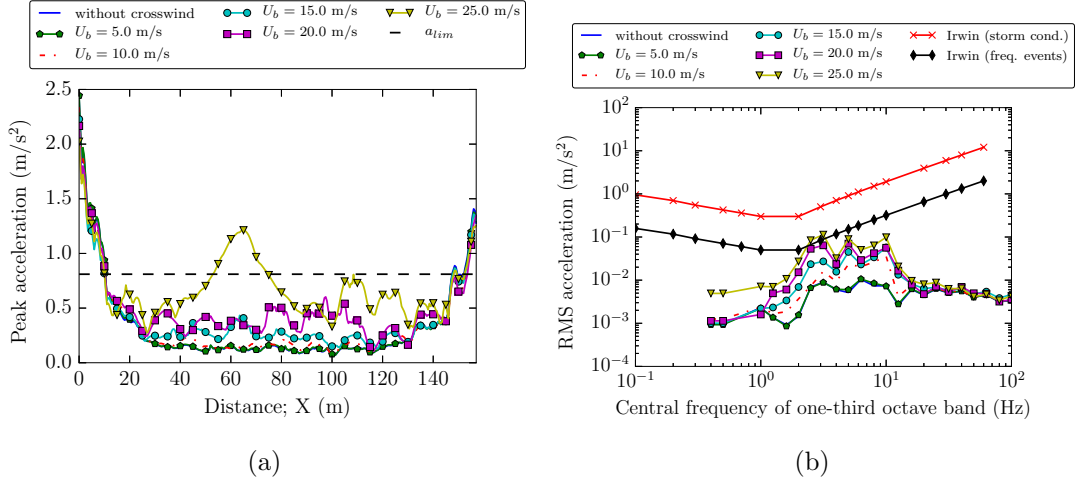


FIG. 9. Effects of crosswind on the vertical vibration of the bridge at $v=100$ km/h: (a) Peak acceleration along sidewalk, (b) RMS acceleration in one-third octave frequency bands at point C_1

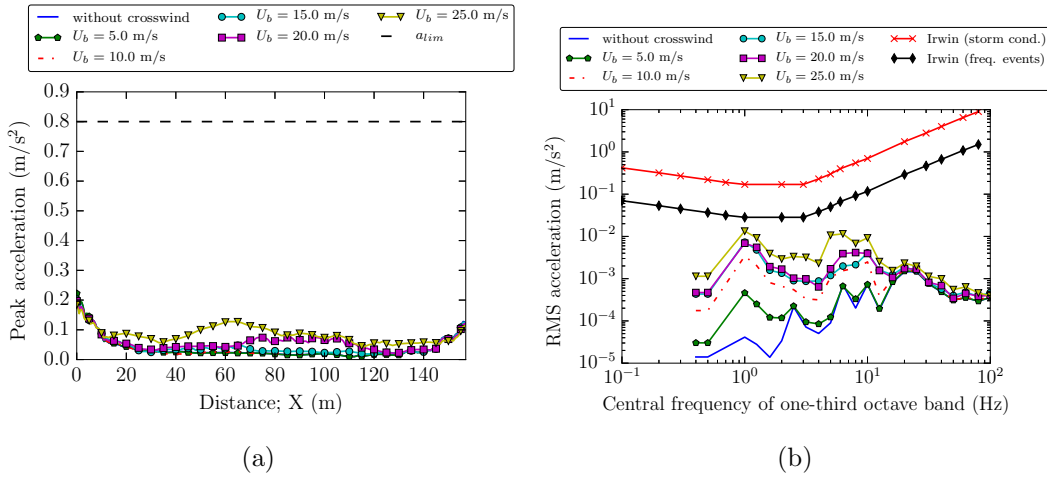


FIG. 10. Effects of crosswind on the lateral vibration of the bridge at $v=100$ km/h: (a) Peak acceleration along sidewalk, (b) RMS acceleration in one-third octave frequency bands at point C_1 .

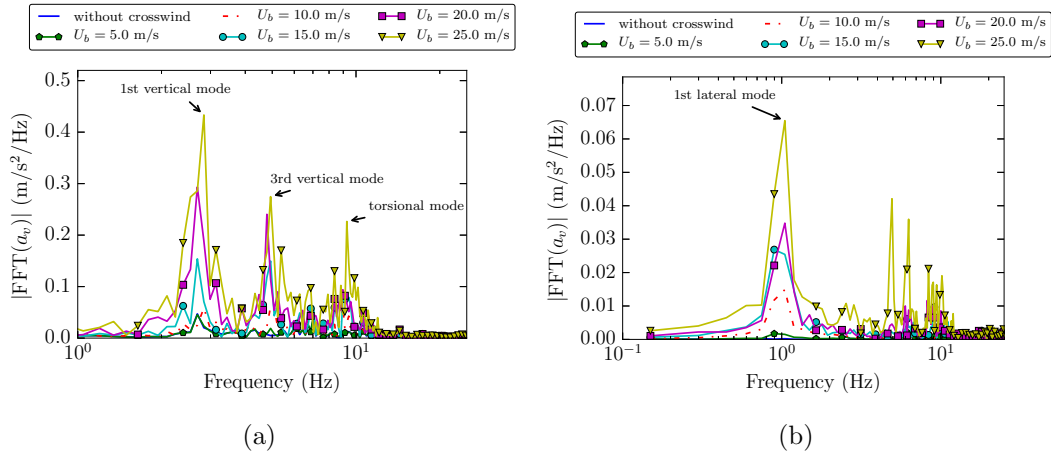


FIG. 11. Frequency content of deck acceleration at point C_1 when the vehicle runs over the bridge at $V = 100$ km/h: (a) vertical acceleration, (b) lateral acceleration.

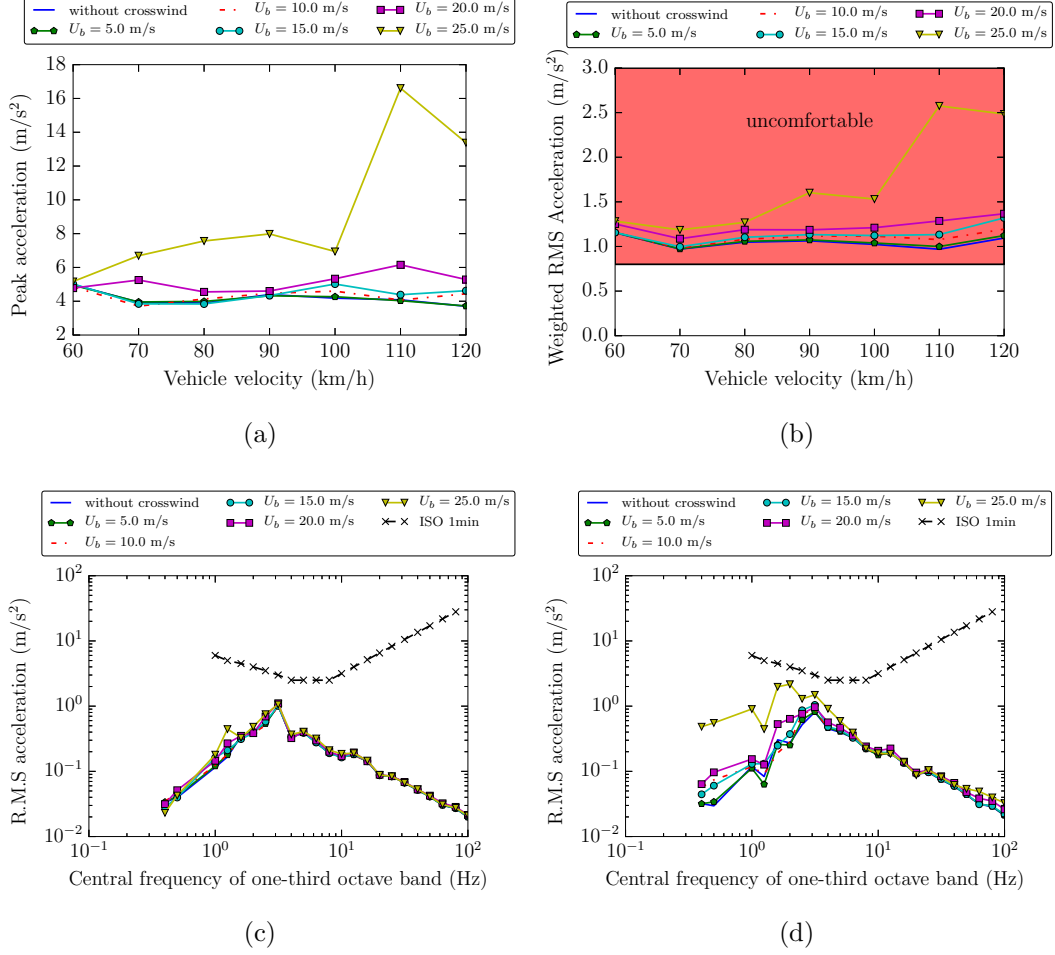


FIG. 12. Vertical vibration of the vehicle: (a) Peak acceleration, (b) Weighted RMS acceleration, (c) Fatigue curve for $V = 60$ km/h, (d) Fatigue curve for $V = 120$ km/h

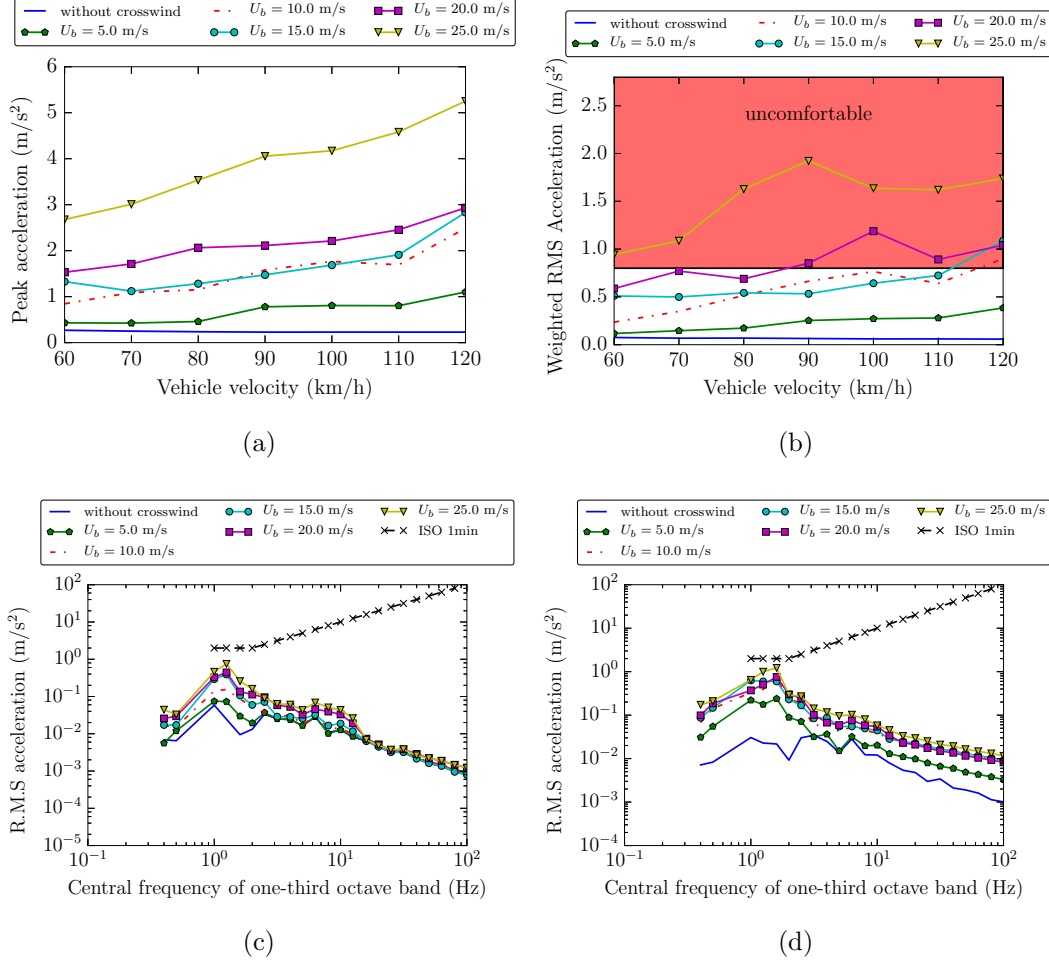


FIG. 13. Lateral vibration of the vehicle: (a) Peak acceleration, (b) Weighted RMS acceleration, (c) Fatigue curve for $V = 60 \text{ km/h}$, (d) Fatigue curve for $V = 120 \text{ km/h}$

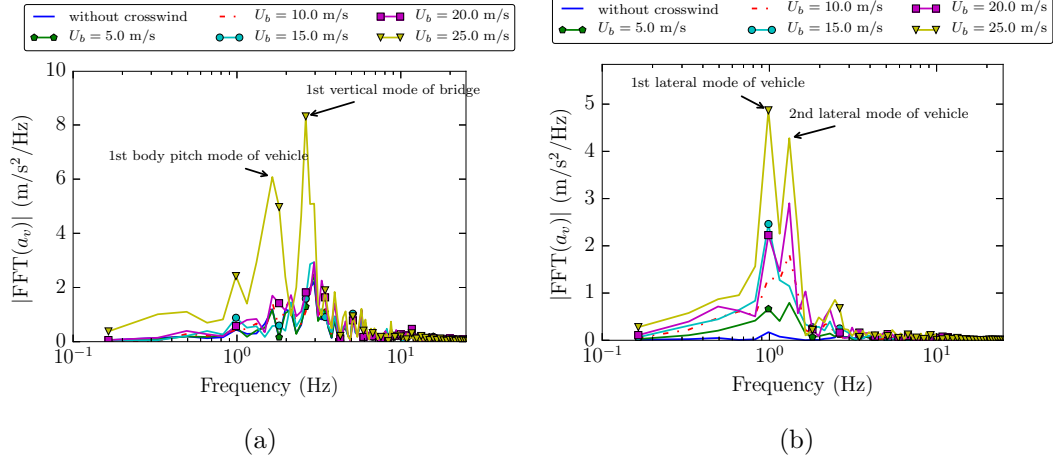


FIG. 14. Frequency content of the acceleration at driver's seat when the vehicle runs over the bridge at $V = 110$ km/h: (a) vertical acceleration, (b) lateral acceleration.

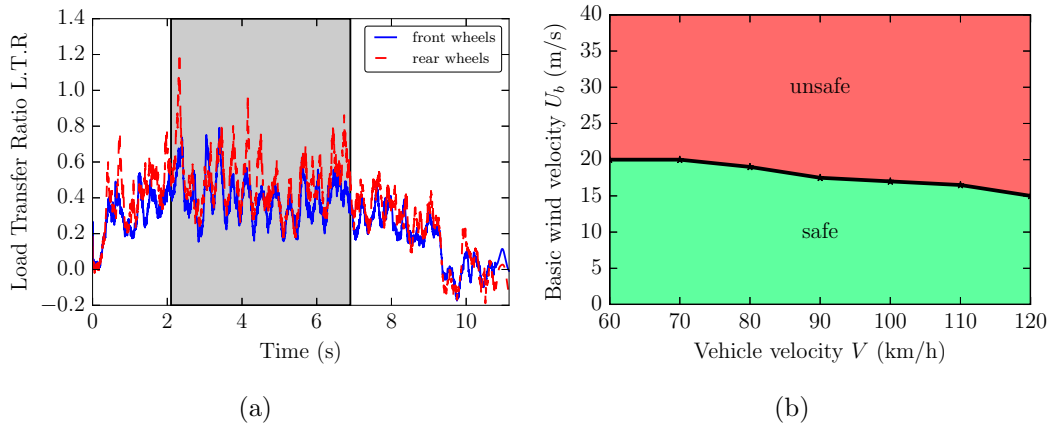


FIG. 15. Vehicle overturning accident assessment: (a) Load Transfer Ratio for $U_b = 20.0$ m/s and $V = 60$ km/h, (b) Critical Wind Curve

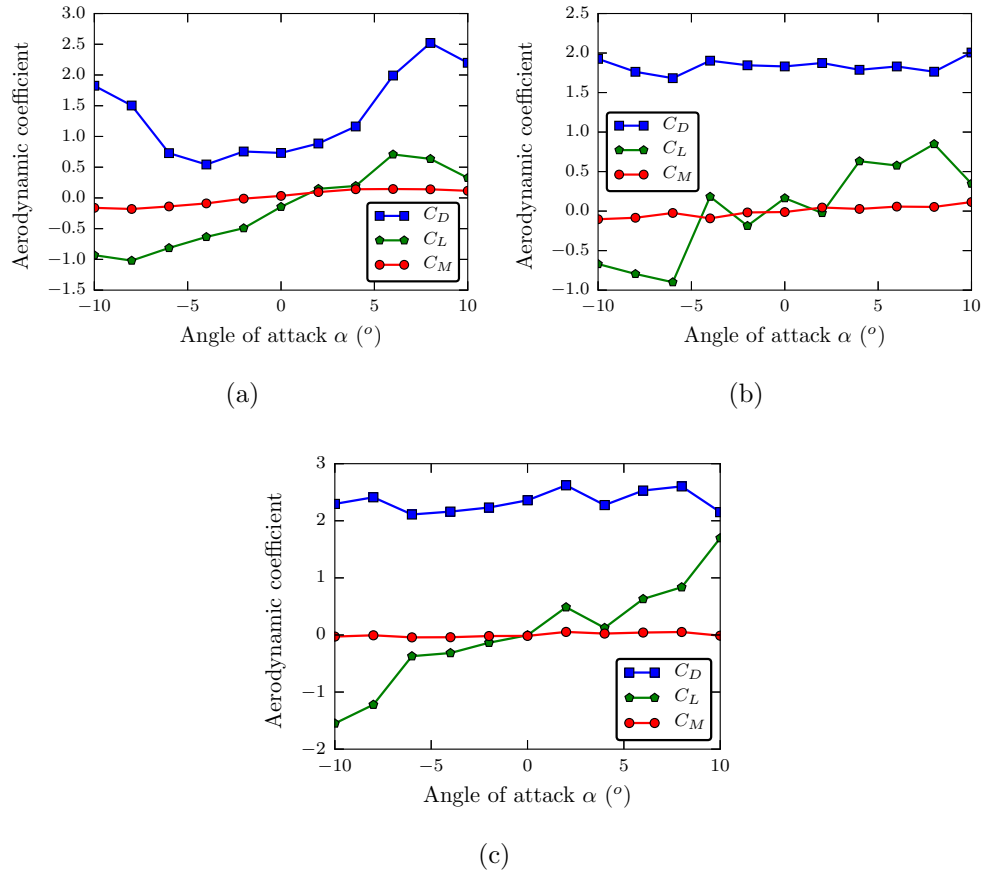


FIG. 16. Aerodynamic coefficients of bridge elements: (a) deck, (b) arch, (c) pier

TABLE 1. Main characterization of parameters of the numerical model of Wild bride

Notation	Parameter	Unit	Adopted and/or updated value	References
E_a	Elastic modulus of arches	GPa	53.3	(Nguyen et al. 2015)
ρ_a	Mass density of arches	kg/m ³	2590	(JCSS 2001a; Kühne and Orgass 2009)
E_p	Elastic modulus of bridge piers	GPa	41.4	(Nguyen et al. 2015)
ρ_p	Mass density of bridge piers	kg/m ³	2500	(JCSS 2001a)
E_d	Elastic modulus of deck	GPa	38.0	(Nguyen et al. 2015)
ρ_d	Mass density of deck	kg/m ³	2518.7	(Nguyen et al. 2015)
m_d	Nonstructural mass on deck	kg/m ²	216.0	(JCSS 2001a)
h_d	Thickness of deck	m	0.601	(Nguyen et al. 2015)
E_{eb}	Bulk modulus of the bearing	GPa	834	(JCSS 2001b)

TABLE 2. Summary of first six modes of vibration of the bridge

Mode	Frequency (Hz)	Description
1	0.874	1st lateral bending
2	2.371	2nd lateral bending
3	2.586	1st vertical bending
4	2.895	2nd vertical bending
5	3.971	3rd vertical bending
6	4.607	3rd lateral bending

TABLE 3. Main parameters of the high-sided truck

Notation	Parameter	Value
m_c	Mass of truck body (kg)	4480
J_{cy}	Pitching moment of inertia of track body (kg.m ²)	5516
J_{cx}	Rolling moment of inertia of track body (kg.m ²)	1349
J_{cz}	Yawing moment of inertia of track body (kg.m ²)	100000
$m_{r,i}$ ($i = 1, 2$)	Mass of rear axle set(kg)	710
$m_{f,i}$ ($i = 1, 2$)	Mass of front axle set(kg)	800
$k_{z,si}$ ($i = 1, 2, 3, 4$)	Vertical stiffness of suspension along Z axis (kN/m)	399
$k_{y,si}$ ($i = 1, 2, 3, 4$)	Lateral stiffness of suspension along Z axis (kN/m)	299
$c_{z,si}$ ($i = 1, 2$)	Vertical damping of rear suspension along Z axis (kN s/m)	5.18
$c_{y,si}$ ($i = 1, 2$)	Lateral damping of rear suspension along Z axis (kN s/m)	5.18
$c_{z,si}$ ($i = 3, 4$)	Vertical damping of front suspension along Z axis (kN s/m)	23.21
$c_{y,si}$ ($i = 3, 4$)	Lateral damping of front suspension along Z axis (kN s/m)	23.21
$k_{z,fi}$ ($i = 1, 2$)	Vertical stiffness of front tire (kN/m)	351
$k_{z,ri}$ ($i = 1, 2$)	Vertical stiffness of rear tire (kN/m)	351
$k_{y,fi}$ ($i = 1, 2$)	Lateral stiffness of front tire (kN/m)	121
$k_{y,ri}$ ($i = 1, 2$)	Lateral stiffness of rear tire (kN/m)	121
$c_{z,fi}$ ($i = 1, 2$)	Vertical damping of front tire (kN s/m)	0.80
$c_{z,ri}$ ($i = 1, 2$)	Vertical damping of rear tire (kN s/m)	0.80
$c_{y,fi}$ ($i = 1, 2$)	Lateral damping of front tire (kN s/m)	0.80
$c_{y,ri}$ ($i = 1, 2$)	Lateral damping of rear tire (kN s/m)	0.80
l_1	Distance (m)	3.0
l_2	Distance (m)	5.0
l_3	Distance (m)	2.7
b_1	Distance (m)	1.10
b_2	Distance (m)	0.80
h_2	Distance (m)	1.30
A_f	Reference area (m ²)	10.5
h_f	Reference height (m)	1.5

List of figure captions

- Figure 1: Exposure limits, fatigue-decreased proficiency boundaries and reduced comfort boundaries to whole-body vibrations given in ISO 2631:1978 (adapted from Handbook of Human Vibration, M. J. Griffin ([Griffin 1990](#)), Chapter 10 Whole-body Vibration Standards, 415–451, Copyright 1990, with permission from Elsevier)

- 671 • Figure 2: Wild Bridge: (a) general view (taken by L. Sparowitz), (b) cross
672 section, (c) knee node
- 673 • Figure 3: High-sided vehicle model in dynamic analysis: (a) side view, (b)
674 front view
- 675 • Figure 4: Simulated wind speed: (a) Position of 53 points for wind speed
676 time histories, (b) Turbulent wind speed at different points for $U_b = 10.0$
677 m/s
- 678 • Figure 5: Relative wind velocity to the running vehicle
- 679 • Figure 6: Diagram of turbulent crosswind actuating on bridge elements
- 680 • Figure 7: User element for modelling the aeroelastic wind forces
- 681 • Figure 8: Load case considered in this study: (a) cross section, (b) plan
682 view and elevation of the bridge, including some control points employed
683 to refer the ongoing results
- 684 • Figure 9: Effects of crosswind on the vertical vibration of the bridge at
685 $v=100$ km/h: (a) Peak acceleration along sidewalk, (b) RMS acceleration
686 in one-third octave frequency bands at point C_1
- 687 • Figure 10: Effects of crosswind on the lateral vibration of the bridge at
688 $v=100$ km/h: (a) Peak acceleration along sidewalk, (b) RMS acceleration
689 in one-third octave frequency bands at point C_1
- 690 • Figure 11: Frequency content of deck acceleration at point C_1 when the
691 vehicle runs over the bridge at $V = 100$ km/h: (a) vertical acceleration, (b)
692 lateral acceleration

- 693 • Figure 12: Vertical vibration of the vehicle: (a) Peak acceleration, (b)
694 Weighted RMS acceleration, (c) Fatigue curve for $V = 60$ km/h, (d) Fatigue
695 curve for $V = 120$ km/h

- 696 • Figure 13: Lateral vibration of the vehicle: (a) Peak acceleration, (b)
697 Weighted RMS acceleration, (c) Fatigue curve for $V = 60$ km/h, (d) Fatigue
698 curve for $V = 120$ km/h

- 699 • Figure 14: Frequency content of the acceleration at driver's seat when the
700 vehicle runs over the bridge at $V = 110$ km/h: (a) vertical acceleration, (b)
701 lateral acceleration

- 702 • Figure 15: Vehicle overturning accident assessment: (a) Load Transfer Ra-
703 tio for $U_b = 20.0$ m/s and $V = 60$ km/h, (b) Critical Wind Curve

- 704 • Figure 16: Aerodynamic coefficients of bridge elements: (a) deck, (b) arch,
705 (c) pier